Check for updates

View Article Online
View Journal

JAAS
Journal of Analytical Atomic Spectrometry

Accepted Manuscript

This article can be cited before page numbers have been issued, to do this please use: A. L. L. M. Souza, M. Aramendía, E. Garcia-Ruiz, F. V. Nakadi, J. Resano and M. Resano, *J. Anal. At. Spectrom.*, 2026, DOI: 10.1039/D6JA00062B.

This is an Accepted Manuscript, which has been through the Royal Society of Chemistry peer review process and has been accepted for publication.

Accepted Manuscripts are published online shortly after acceptance, before technical editing, formatting and proof reading. Using this free service, authors can make their results available to the community, in citable form, before we publish the edited article. We will replace this Accepted Manuscript with the edited and formatted Advance Article as soon as it is available.

You can find more information about Accepted Manuscripts in the Information for Authors.

Please note that technical editing may introduce minor changes to the text and/or graphics, which may alter content. The journal's standard Terms & Conditions and the Ethical guidelines still apply. In no event shall the Royal Society of Chemistry be held responsible for any errors or omissions in this Accepted Manuscript or any consequences arising from the use of any information it contains.

ROYAL SOCIETY OF CHEMISTRY

rsc.li/jaas

View Article Online
DOI: 10.1039/D6JA00062B

Single- and dual-isotopic analysis using high-resolution continuum-source graphite-furnace molecular absorption. Strategies for data selection, processing, and modeling

André L. M. de Souza,[a] Maite Aramendía,[a]* Esperanza García-Ruiz,[a] Flávio V. Nakadi,[a] Javier Resano,[b] Martín Resano[a]*

[a] Department of Analytical Chemistry, Aragon Institute of Engineering Research (I3A), University of Zaragoza, Pedro Cerbuna 12, 50009 Zaragoza, Spain.

[b] University of Zaragoza, Department of Computer Science and Systems Engineering, Aragon Institute of Engineering Research (I3A), Zaragoza, 50018, Spain

*Corresponding author: mresano@unizar.es; maiteam@unizar.es

Open Access Article. Published on 23 April 2026. Downloaded on 4/23/2026 9:19:50 PM.
This article is licensed under a Creative Commons Attribution-NonCommercial 3.0 Unported Licence.

Abstract

This work evaluates different strategies for data processing, aiming at achieving isotopic information *via* high-resolution continuum-source graphite-furnace molecular absorption. For this purpose, two different molecules are investigated: CaF and CaCl. In the first case, only the measurement of ^{44}Ca and ^{40}Ca is pursued, whereas in the second case, isotopic variations affect both elements present in the molecule (^{44}Ca and ^{40}Ca, but also ^{37}Cl and ^{35}Cl). Thus, two different approaches are proposed.

For Ca isotopic analysis through the monitoring of CaF, the effects of selecting the number of detection pixels and the number of molecular spectra, as well as of using a regression approach for temporal data, are discussed. Overall, using three detector pixels and using this regression approach tend to produce the best results (0.5-1.0% RSD) for isotopic analysis *via* HR CS GFMAS in those situations in which the signal can be derived from two separate peaks.

On the other hand, to perform simultaneous Ca and Cl isotopic analysis by monitoring CaCl, a machine-learning strategy is proposed. The performance of such a model is

Journal of Analytical Atomic Spectrometry Accepted Manuscript

View Article Online
DOI: 10.1039/D6JA00062B

promising for isotopic abundances of at least 10% (median absolute percentage error of 1.21%), while the error escalates when one of the isotopes shows a lower abundance. To detect such underperforming situations in real-world settings, it is recommended to monitor the prediction uncertainty to set thresholds and flag results with poor reliability.

Open Access Article. Published on 23 April 2026. Downloaded on 4/23/2026 9:19:50 PM.
This article is licensed under a Creative Commons Attribution-NonCommercial 3.0 Unported Licence.

Journal of Analytical Atomic Spectrometry Accepted Manuscript

View Article Online
DOI: 10.1039/D6JA00062B

1. Introduction

Among other key advantages, the use of high-resolution instrumentation has enabled the monitoring of well-resolved molecular spectra with traditionally atomic sources.[1,2] This has opened up new possibilities for monitoring elements that are difficult to measure using atomic techniques (e.g., non-metals).[3–5] Literature on this topic using high-resolution continuum source molecular absorption spectrometry (HR CS MAS) in either flame (F) or graphite furnace (GF) atomizers is extensive,[6,7] but other techniques, such as laser-induced breakdown spectroscopy (LIBS), have also benefited from these opportunities.[1,8]

Monitoring molecular spectra with sufficient resolution also offers new opportunities to access isotopic information, because the isotopic shifts in molecular spectra are significantly larger than those in their atomic counterparts. This approach was first explored for LIBS, giving rise to laser ablation molecular isotopic spectrometry (LAMIS),[9-11] and was later also evaluated for HR CS GFMAS, which, among other aspects, may offer superior sensitivity, although with much more limited multi-element potential.

Despite the obvious interest in getting access to a new type of information (isotopic) for techniques traditionally restricted to elemental analysis, except for the very few elements (e.g., B or Li) for which the isotopic atomic transitions are sufficiently resolved,[12,13] only a few papers to date have been published making use of isotopic analysis *via* HR CS GFMAS.

Our research group reported on the first work on this topic in 2015, demonstrating the separate monitoring of $Al^{35}Cl$ and $Al^{37}Cl$ transitions,[14] thus enabling Cl isotopic monitoring. Two distinct peaks for these species were observed under optimized conditions, and precision values of around 2% RSD for Cl content at the mg L^{-1} level

Open Access Article. Published on 23 April 2026. Downloaded on 4/23/2026 9:19:50 PM.
This article is licensed under a Creative Commons Attribution-NonCommercial 3.0 Unported Licence.

Journal of Analytical Atomic Spectrometry Accepted Manuscript

View Article Online
DOI: 10.1039/D6JA00062B

were reported. Furthermore, the potential of using isotope dilution for mitigating chemical interferences when determining Cl in mineral water was demonstrated.

In a later work, a similar strategy was applied to obtain Br isotopic information. After evaluating various molecule-forming agents, Ca was selected, enabling the selective monitoring of $Ca^{79}Br$ and $Ca^{81}Br$ transitions.[15] The precision obtained was around 2.5% RSD for 10 mg L^{-1} Br aqueous solutions. It was shown that the method can also be applied directly to solid samples, where the use of isotope dilution permitted the direct determination of Br in PVC and tomato leaves reference materials, despite the chemical interferences detected.

Isotopic analysis of B, based on measurements of the ^{10}BH and ^{11}BH transitions, was then demonstrated by Abad et al. by monitoring transitions around wavelengths 433.1 nm and 437.1 nm.[16] Excellent precision was achieved (with expanded uncertainties in the 0.015-0.044% range) by building a spectral library with different isotope ratios for partial least square regression (PLSR), but only for concentrations of at least 1 g L^{-1}. Still, this indicates that the use of more advanced chemometric tools can help in improving precision for HR CS GFMAS isotopic analysis, in the same way as is common for LAMIS,[8,10,11] where, for instance, the use of PLSR is very usual. It makes sense to assume that such tools are particularly important for maximizing the information obtained from complex, rich spectra. Even more so since other common strategies applied in LAMIS to improve precision, such as the accumulation of spectra, can hardly be applied to HR CS GFMAS.

The selective monitoring of ^{40}CaF and ^{44}CaF was reported by Zanatta et al.[17] This work, rather than measuring isotopic ratios, focused on determining ^{40}Ca and ^{44}Ca isotopes in urine samples, after Ca separation by precipitation with ammonium oxalate to remove Cl interference. It can be mentioned that the $A^2\Pi - X^2\Sigma+$ band of CaF

Open Access Article. Published on 23 April 2026. Downloaded on 4/23/2026 9:19:50 PM.
This article is licensed under a Creative Commons Attribution-NonCommercial 3.0 Unported Licence.

Journal of Analytical Atomic Spectrometry Accepted Manuscript

View Article Online
DOI: 10.1039/D6JA00062B

isotopologues has been investigated in detail recently by means of laser-induced fluorescence spectroscopy.[18]

Bazo et al. expanded the field by reporting data on the four stable isotopes of Sr (by measuring ^{88}SrF, ^{87}SrF, ^{86}SrF, and ^{84}SrF transitions), rather than only two as in previous works.[19] To overcome spectral overlap, a deconvolution approach was used. The reported precision for isotope ratios was relatively high (6-11% RSD), but the approach demonstrated potential for monitoring ^{84}Sr as a tracer in tap water.

Aramendía et al. explored the formation of BF with a double purpose: i) to enable the determination of B using a milder temperature program, thus improving the potential for measuring this refractory element in a graphite furnace; ii) to attain isotopic information. In this regard, it was possible to calculate ^{11}B/^{10}B ratios by separately monitoring the ^{11}BF and ^{10}BF molecular absorption transitions, with RSD values improving for higher B masses, but only down to 3-4 % under the best conditions.[20]

Finally, Abad et al. monitored ^{14}NO and ^{15}NO transitions and developed an isotope-dilution-based method for determining total nitrate + nitrite in natural waters.[21] The transitions of the isotopologues overlap partially, so non-linear multivariate analysis (PLSR) was required for spectral deconvolution. The expanded uncertainty reached 2-4% RSD.

Therefore, the number of articles published on this topic over the last ten years remains rather limited. This could be, among other reasons, because the optical community is not accustomed to the concept of isotopic analysis, its potential, and the methods for maximizing the information it can yield. But perhaps most importantly, there remains a lack of understanding of fundamental aspects, including the primary sources of uncertainty.

Open Access Article. Published on 23 April 2026. Downloaded on 4/23/2026 9:19:50 PM.
This article is licensed under a Creative Commons Attribution-NonCommercial 3.0 Unported Licence.

Journal of Analytical Atomic Spectrometry Accepted Manuscript

View Article Online
DOI: 10.1039/D6JA00062B

Open Access Article. Published on 23 April 2026. Downloaded on 4/23/2026 9:19:50 PM.
This article is licensed under a Creative Commons Attribution-NonCommercial 3.0 Unported Licence.

In this regard, it may be difficult to disentangle some of these potential sources of uncertainty (e.g., possible temporal variations superimposed on noise). Nevertheless, from a practical point of view, it is at least possible to investigate the optimal data processing approaches required to improve data quality. Furthermore, as discussed above, the RSD values reported *via* HR CS GFMAS in the vast majority of cases are of a few %. This may suffice for some applications (e.g., isotope dilution or tracer experiments), but not for others (e.g., monitoring natural variations), and leaves room for improvement.

This work further explores new approaches to data treatment in order to obtain results of the highest analytical quality. For this purpose, two different molecules are investigated *via* HR CS GFMAS, namely CaF and CaCl. Such molecules are selected because they correspond to two very different situations.

CaF offers a relatively simple isotopic system, in which the only possible isotopic variations stem from one of the elements composing the molecule (Ca). The best strategy for the selection of the most representative portion of the 3D signals generated *via* HR CS GFMAS will be investigated. Special attention will be paid to the translation of the regression approach, originally developed for the treatment of transient isotopic signals with multicollector inductively coupled plasma mass spectrometry (MC-ICP-MS),[22,23] to HR CS GFMAS isotopic analysis. It should be noted that, since the goal differs from that explored by Zanatta et al.[17,] which was a tracer experiment, different transitions will be monitored.

CaCl, on the other hand, has been selected to represent a more complex situation in which both elements show a potential isotopic variation. The resulting spectra are significantly more complex in terms of lines, and a novel approach based on machine

Journal of Analytical Atomic Spectrometry Accepted Manuscript

View Article Online
DOI: 10.1039/D6JA00062B

learning is tested to predict the isotopic compositions of both Ca and Cl simultaneously.

Finally, we consider it necessary to clarify that this is a proof-of-concept study focused on achieving the best analytical performance from model solutions, unlike previous works where analysis of real samples was demonstrated, as discussed before.

2. Experimental

2.1. Instrumentation

The absorption experiments were performed using an HR CS atomic absorption spectrometer ContrAA 800G (Analytik Jena, Germany), equipped with a transversely heated graphite tube, an Xe short-arc lamp, and an autosampler for solution samples. The Ca isotopic compositions were validated using an inductively coupled plasma mass spectrometer NexION 5000 (PerkinElmer, USA) operated in ICP-MS/MS mode, with NH_3 (Nippon Gases, Spain) as the reaction gas.

2.2. Solutions and reagents

All reagents used in the work were of analytical grade or higher. Deionized water (18 MΩ·cm) obtained from a Milli-Q water system (Millipore, France) was used for dilutions throughout the work, with nitric acid (Merck, Germany) when indicated.

For CaF molecule studies, calcium standards with different isotopic compositions were used. A 1000 mg L^{-1} Ca standard solution (Merck, Germany) was used for the natural stock (^{40}Ca abundance of 96.9%). A 1000 mg L^{-1} ^{44}Ca-enriched solution (certified ^{44}Ca atomic abundance of 99.2%) was prepared from the $CaCO_3$ salt (Neonest AB, Sweden) dissolved in a 1% HNO_3 (v v^{-1}) solution. As the fluorinating agent, a NaF (Merck, Germany) 5% (m v^{-1}) solution was prepared.

For CaCl studies, in addition to the Ca standards previously described, a 1000 mg L^{-1} Cl standard solution (Merck, Germany) was used as a reference for natural abundance

Open Access Article. Published on 23 April 2026. Downloaded on 4/23/2026 9:19:50 PM.
This article is licensed under a Creative Commons Attribution-NonCommercial 3.0 Unported Licence.

Journal of Analytical Atomic Spectrometry Accepted Manuscript

View Article Online
DOI: 10.1039/D6JA00062B

(^{35}Cl, 75.8% and ^{37}Cl, 24.2%, respectively). A ^{35}Cl-enriched NaCl salt (CortecNet, France) with certified abundance of 99.1% was dissolved in a HNO_3 1% v v^{-1} solution for a final Cl concentration of approximately 200 mg L^{-1}. Finally, a 164.6 mg L^{-1} ^{37}Cl-enriched standard (ERM, Belgium) with a certified ^{37}Cl atomic abundance of 98.1% was also measured.

2.3. Procedure for monitoring CaF via HR CS GFMAS

The CaF molecule was observed by its $B^2\Sigma$-$X^2\Sigma$ (ν'=2 and ν''=1, respectively) transition, found in the vicinity of 515.3 nm,[24] with the spectra centered at 515.350 nm at pixel 101, and the spectral window covering the range between 515.023-515.673 nm with 200 pixels. As shown in **Figure 1**, this spectral window presents four peak profiles: two peaks for ^{40}CaF centered at pixels 52 and 81 (515.190 and 515.284 nm, respectively), and the other two peaks for ^{44}CaF centered at pixels 119 and 149 (515.408 and 515.503 nm, respectively). The baseline signal was fixed using the IBC-m mode. The peaks at pixels 52 and 119 were ultimately selected, and each of them is characterized by up to 19 detector pixels (spectral resolution) and 20 data points (temporal resolution).

For each measurement, 10 μL of a Ca solution of different concentrations that varied from 200 to 1000 mg L^{-1} (2 to 10 μg of total calcium, respectively) was deposited into the furnace, together with 10 μL of NaF 5% (m v^{-1}) solution as a fluorinating agent. The calcium isotopic compositions also varied: ^{44}Ca/^{40}Ca ratios of 4:1, 1:1, and 1:4 were measured. The measurements were done using the liquid autosampler, and no chemical modifier was used. The furnace program used was adapted from prior work[17] and is presented in **Table 1**. For each calcium concentration and isotopic composition, 15 measurements were carried out. Additionally, 10 measurements of a blank solution

Open Access Article. Published on 23 April 2026. Downloaded on 4/23/2026 9:19:50 PM.
This article is licensed under a Creative Commons Attribution-NonCommercial 3.0 Unported Licence.

Journal of Analytical Atomic Spectrometry Accepted Manuscript

View Article Online
DOI: 10.1039/D6JA00062B

containing only the fluorinating agent were performed. The final spectrum for each measurement was corrected by the average of the 10 blank spectra.

2.4. Procedure for monitoring CaCl via HR CS GFMAS

The CaCl molecule was measured at its $A^2\Pi$-$X^2\Sigma$ transition, found in the region of 605.1 nm (ν''=0 and ν'=1, respectively).[24] The 200 pixel spectrum was centered at 604.970 nm (detector pixel 101), and the spectral window covered the range between 604.583 and 605.353 nm. Ca and Cl standard solutions with a final concentration of 180 mg L^{-1} were both measured, introducing 10 μL of each solution into the furnace (1.8 μg for each analyte). For this molecule, both elements exhibit various isotopes, generating four main combinations: $^{44}Ca^{35}Cl$, $^{40}Ca^{35}Cl$, $^{44}Ca^{37}Cl$, and $^{40}Ca^{37}Cl$. The influence of other minor calcium isotopes was not the aim of this study and was not considered.

To observe the spectral variations when both Ca and Cl are mixed, the $^{44}Ca/^{40}Ca$ and $^{37}Cl/^{35}Cl$ isotopic composition were both varied from 0:1 to 1:0, in increments of 10%, resulting in 121 different combinations. The solution for each combination was analyzed 5 times, and a 1% HNO_3 (v v^{-1}) blank solution was measured 10 times. The IBC-m background correction method was also used for this molecule. These measurements were used to build the machine learning model discussed in section 3.3 and were obtained in four different full-day sessions. The experiments for additional validation with unknowns were conducted on a separate day, four weeks after the others.

A 2D (wavelength vs. absorbance) spectrum for each measurement was produced, selecting the temporal spectrum that provides the highest absorbance value (or else, the highest spectrum plus the ones measured before and after; or the highest spectrum plus the two measured before and the two after), always corrected by the

Open Access Article. Published on 23 April 2026. Downloaded on 4/23/2026 9:19:50 PM.
This article is licensed under a Creative Commons Attribution-NonCommercial 3.0 Unported Licence.

Journal of Analytical Atomic Spectrometry Accepted Manuscript

View Article Online
DOI: 10.1039/D6JA00062B

blank spectrum. Finally, all spectra were normalized to their maximum absorbance to reduce variability across different measurement days.

Table 2 displays the instrumental measurement conditions, which were adapted from a previous work.[25]

2.5. Procedure for Ca isotopic analysis via ICP-MS

Ca standards with $^{44}Ca/^{40}Ca$ theoretical isotopic compositions prepared as 4:1, 1:1, and 1:4 were measured using an ICP-MS/MS to assess the real $^{44}Ca/^{40}Ca$ ratio. Solutions were diluted to a final concentration of 200 $\mu g\ L^{-1}$ and analyzed under the following parameters: 16 L min^{-1} plasma Ar gas flow, 1.1 L min^{-1} nebulizer Ar gas flow, 1.01 L min^{-1} auxiliary Ar gas flow, 1.2 mL min^{-1} reaction gas flow (NH_3), and 1600 W RF power. The nuclides monitored were $^{40}Ca^+$ and $^{44}Ca^+$, with both quadrupoles (Q1 and Q3) set to transmit m/z values of 39.9626 and 43.9555, respectively. The dwell time per isotope was 50 ms. Instrumental mass bias was corrected using the natural Ca standard as a reference. Also, a 1% HNO_3 (v v^{-1}) blank solution was measured.

5 replicates were carried out for each isotopic composition, and the uncertainties obtained (expressed as RSD) were: $^{44}Ca/^{40}Ca$ 4:1 (0.58%), $^{44}Ca/^{40}Ca$ 1:1 (0.29%), and $^{44}Ca/^{40}Ca$ 1:4 (0.57%).

3. Results and discussion

3.1. CaF: selecting and processing signal portions

The first case evaluated in this work is the molecule CaF, which can be formed in the gaseous phase with relative ease in a graphite furnace. To achieve this, an excess of fluorinating agent is added, as detailed in section 2.3, and the temperature program shown in **Table 1** is applied.

Under these conditions, there are different CaF transitions that can be monitored and that respond selectively to different Ca isotopes, because the presence of F, being

Open Access Article. Published on 23 April 2026. Downloaded on 4/23/2026 9:19:50 PM.
This article is licensed under a Creative Commons Attribution-NonCommercial 3.0 Unported Licence.

Journal of Analytical Atomic Spectrometry Accepted Manuscript

View Article Online
DOI: 10.1039/D6JA00062B

monoisotopic, does not affect the observed shift. The transition ($B^2\Sigma$-$X^2\Sigma$; $v'=2$, $v''=1$), which shows its main lines around 515.3 nm,[24] was selected for the study because it offers a clean spectrum with low noise. For simplicity, only the two main calcium isotopes ^{40}Ca and ^{44}Ca (for which a spike is used) are considered, since the abundance of the other Ca isotopes will be too low to show a significant signal for the solutions measured.

Figure 1 shows an example of the type of signal that is obtained under these conditions. As is typical of HR CS GFMAS, it is a 3D signal, where each one of the detector pixels (X-axis) monitors a particular wavelength (with a resolution of roughly 3.25 pm in this spectral range). The signal is obviously transient in nature (Y-axis), and the absorbance (Z-axis) of the whole spectrum is recorded approximately every 0.073 s. 2D signals (normalized absorbance vs. wavelength; normalized absorbance vs. time) are also projected onto the sides of the figure, allowing for a better appreciation of the effects of time and wavelength on the signal.

As shown in this figure, there are actually two doublets that respond selectively to ^{40}CaF and ^{44}CaF. Their sensitivities are very similar, so the results will focus on the first one from now on. The shift between these ^{40}CaF and ^{44}CaF signals is rather large (218 pm, corresponding to 67 detector pixels). The shift predicted for this transition, using the theoretical equations discussed in detail elsewhere,[14,26] is 203.8 pm.

Unlike the situation for elemental analysis, there is no clear protocol to obtain isotopic information of the best quality from these signals. However, as is known from other high-precision isotopic techniques that use transient signals (e.g., when a laser ablation (LA) device is coupled to MC-ICP-MS), selecting the entire signal can degrade precision.

Open Access Article. Published on 23 April 2026. Downloaded on 4/23/2026 9:19:50 PM.
This article is licensed under a Creative Commons Attribution-NonCommercial 3.0 Unported Licence.

Journal of Analytical Atomic Spectrometry Accepted Manuscript

View Article Online
DOI: 10.1039/D6JA00062B

Open Access Article. Published on 23 April 2026. Downloaded on 4/23/2026 9:19:50 PM.
This article is licensed under a Creative Commons Attribution-NonCommercial 3.0 Unported Licence.

This situation can also be inferred for HR CS GFMAS signals, as shown in **Figures 2** and **3**. **Figure 2** shows the effect of the number of detector pixels selected (thus, the wavelength range covered). As shown in the figure, for both ^{40}CaF (**Figure 2a**) and ^{44}CaF (**Figure 2b**), signal imprecision (evaluated as the RSD of 15 measurements) increases sharply for pixels with lower absorption, as expected and previously described.[27] This has a direct consequence for the measurement of the ^{44}Ca/^{40}Ca ratio (see **Figure 2c**), as the best precision (together with a ratio close to the expected value for this experiment, which is 1) is obtained only by ratioing the four central pixels. Obviously, adding more pixels increases noise due to the lower absorbance signal, which detracts from data quality. Thus, in this regard, the situation is similar to when trace elemental analysis is targeted *via* HR CS GFMAS/AAS, and the optimal number of pixels falls within the typically recommended 3-5 value.[27,28]

However, the influence of the other dimension (time) has not been evaluated as systematically in HR CS GFMAS/AAS measurements. Not for elemental analysis, where the whole signal is usually time-integrated, and even less so for isotopic analysis. Still, the influence on the quality of the results is very similar to that shown for the detector pixels. As shown in **Figure 3**, the signals for both ^{40}CaF (**Figure 3a**) and ^{44}CaF (**Figure 3b**) exhibit significantly higher RSD values when considering the start or tail of the signals. And this imprecision ultimately affects the measurement of the ^{44}Ca/^{40}Ca ratio (see **Figure 3c**). Achieving good precision is only possible when just the central part of the signal is considered, due to a better signal-to-noise ratio.

Now, defining the number of spectra to consider is not so straightforward as for the detector pixels. It is much more difficult to generalize when discussing the transient nature of the HR CS GFMAS signals because the contribution of the tailing to the total signal varies for different molecules. Very volatile ones will hardly exhibit any tailing,

Journal of Analytical Atomic Spectrometry Accepted Manuscript

View Article Online
DOI: 10.1039/D6JA00062B

whereas refractory ones will do. It is therefore not simple to establish a rule, and it will *a priori* be desirable to find a way to use all of the spectra, to avoid subjectivity, while at the same time avoiding the extra uncertainty induced by those signal portions of lower absorbance.

This situation has already been explored for MC-ICP-MS when using sample introduction systems that produce transient signals, as discussed in the introduction. The elegant solution proposed was to leverage the properties of linear regression.[22,23] If all the spectral points are used to calculate the ratios and then plotted for a least-squares linear regression, the slope of the plot will correspond to the estimated ratio. However, in such a regression, not all points contribute equally to the resulting equation, as it is well known that higher values carry greater weight. This approach may, therefore, also be recommendable in HR CS GFMAS.

Figure 4 illustrates how this method works in practice and demonstrates that a high-quality regression model is obtained for the ^{40}CaF and ^{44}CaF signals, thereby offering a new approach to data processing.

3.2. CaF: key factors affecting the quality of isotopic analysis data

In order to further study the main parameters affecting the quality of the isotopic information, and keeping the ideas discussed in the previous section in mind, a systematic study was carried out varying the number of detector pixels used, the portion of the transient signal considered, including the possibility of using it completely with the regression approach, and also varying the ^{40}Ca and ^{44}Ca ratios, as well as the total Ca concentration. The results obtained are shown in **Figure 5**.

As can be seen in that figure (**Figure 5a**), when the ratio is 1:1, the best precision is attained, as expected. For such a ratio, precision values of 0.5% to 1.0% RSD are typically achieved in most cases, regardless of concentration. The approach selected

Open Access Article. Published on 23 April 2026. Downloaded on 4/23/2026 9:19:50 PM.
This article is licensed under a Creative Commons Attribution-NonCommercial 3.0 Unported Licence.

Journal of Analytical Atomic Spectrometry Accepted Manuscript

View Article Online
DOI: 10.1039/D6JA00062B

for data processing in this most favorable case seems less relevant. Still, some of the 2-factor (number of detector pixels, mode of processing the transient signal) ANOVAs carried out indicated differences that were statistically significant (mode of processing the transient signal: for 400 mg L^{-1} and 600 mg L^{-1}; number of detector pixels: for 600, 800, and 1000 mg L^{-1}). The best precision values are obtained overall with 3 detector pixels (average ± standard deviation, 0.59 ± 0.06%) and with the regression approach (0.60 ± 0.57%). However, regarding the way of processing the transient signal, the results are only clearly worse when the maximum value is used (0.82 ± 0.78%).

When the ratio is not so favorable, precision degrades, as could be anticipated. In general, the measurement of an isotope found at a lower level can be potentially more affected by noise variations, particularly since the definition of the baseline would be primarily influenced by the highest signals. In these situations (see **Figure 5b** and **Figure 5c**), the role of concentration becomes very clear, and precision degrades significantly at Ca contents of 200 and 400 mg L^{-1}, hinting at low signal-to-noise ratios for the less abundant isotope. The potential effect of non-linearity for high signals does not seem to affect precision. However, this effect may affect the accuracy of the ratio, as will be discussed later.

In particular, for the $^{44}CaF/^{40}CaF$ ratio of approx. 0.25, ANOVAs found significant differences related to the number of detector pixels in all cases, and also regarding the mode of processing the signals for 400 and 1000 mg L^{-1}. In practice, the difference between selecting 3 or 5 detector pixels per peak is minimal (1.09 ± 0.55% for 3 pixels; 1.13 ± 0.60% for 5 pixels), but again, using only one pixel (2.24 ± 0.66%) is not recommended. The difference between using the regression approach or 3 or 5 peak points is practically negligible (1.42 ± 1.24% for regression; 1.43 ± 1.27% for 3 points; 1.40 ± 1.25% for 5 points), but both using the maximum peak point (1.56 ± 1.37%) or

Open Access Article. Published on 23 April 2026. Downloaded on 4/23/2026 9:19:50 PM.
This article is licensed under a Creative Commons Attribution-NonCommercial 3.0 Unported Licence.

Journal of Analytical Atomic Spectrometry Accepted Manuscript

View Article Online
DOI: 10.1039/D6JA00062B

the 10 peak points that characterize the whole signal peak (1.63 ± 1.40%), potentially increase the uncertainty.

On the other hand, for the $^{44}CaF/^{40}CaF$ ratio close to 4, the trend is even clearer. ANOVAs found statistical differences in all cases except for one (the way of processing the signals for 600 mg L^{-1}). Best precision is obtained with either 1 (1.04 ± 0.49%) or 3 detector pixels (1.12 ± 0.40%), and it degrades for 5 (1.45% ± 0.76%). Concerning signal processing, the regression approach performs best in the vast majority of cases (1.02 ± 0.90%), and precision degrades as the number of peak points increases, reaching its worst value when 10 peak points are considered (1.50 ± 1.19%).

Overall, based on these precision values, the best conditions (or very close to them) are always achieved with 3 detector pixels and the regression approach, providing values around 1% RSD or better, and around 0.5% in the most favorable situations (ratio close to 1). While these values may still not be sufficiently good to monitor Ca natural variations, they represent an improvement over previous results reported for isotopic analysis *via* HR CS GFMAS (see introduction), which were most often around 2-3% RSD, or even higher.

Finally, while the primary goal of this work is to establish the optimal way to process the data to reduce uncertainty, it is obviously important to provide ratios as accurately as possible. To further evaluate this, the solutions prepared as described in section 2 were analyzed by ICP-MS to determine their actual $^{44}Ca/^{40}Ca$ ratio, which served as the reference. The ratio of the calculated to the reference value, for the same dataset used in **Figure 5,** is shown in **Figure 6**.

Again, it is evident that the total concentration significantly affects the result. Nevertheless, it is possible to achieve a value most often within 2% of the expected one for a $^{44}Ca/^{40}Ca$ ratio of approximately 1 or 0.25, and that is without any correction

Open Access Article. Published on 23 April 2026. Downloaded on 4/23/2026 9:19:50 PM.
This article is licensed under a Creative Commons Attribution-NonCommercial 3.0 Unported Licence.

Journal of Analytical Atomic Spectrometry Accepted Manuscript

View Article Online
DOI: 10.1039/D6JA00062B

approaches, as required for other techniques. For instance, when using ICP-MS, the instrumental mass bias for $^{44}Ca/^{40}Ca$ is very high (-23% in our working conditions) and was corrected for using a standard for which the natural abundance was assumed.

On the other hand, the results for a $^{44}Ca/^{40}Ca$ ratio of approximately 4 are less accurate and show a decreasing trend with increasing concentration, approaching the correct value at higher concentrations. This trend (lower ratio with higher concentration) is the inverse of that observed for a $^{44}Ca/^{40}Ca$ ratio of 0.25 and can be at least partially explained by the restricted linear range, which is always a factor to consider when estimating ratios *via* absorption techniques. Again, for $^{44}Ca/^{40}Ca$ ratios close to 4, it is obvious that a lower bias is obtained using the regression approach, and the bias (in the same way as the imprecision) increases as more peak points are included in the signal.

Thus, overall, using 3 detector pixels and using the regression approach is proposed as the most promising approach for deploying HR CS GFMAS for isotopic analysis of those situations in which the signal can be derived from two separate peaks.

3.3. CaCl: Modeling data for dual isotopic analysis

As detailed in section 2.4., the CaCl molecule was measured at its $A^2\Pi$-$X^2\Sigma$ transition ($\nu''=0$, $\nu'=1$).[24] As shown in **Figure 7**, in this case, the location of the peaks depends on the isotopic composition of the CaCl molecule. For instance, peak 1 from $^{40}Ca^{35}Cl$ is measured at detector pixel 27 (604.683 nm), whereas for $^{44}Ca^{37}Cl$, peak 1 is centered at pixel 151 (605.163 nm). There are various CaCl peaks that can be monitored, but only the first five peaks (highlighted in **Figure 7**) can always be detected simultaneously for each possible isotopic combination, given the 200 detector pixels available.

Open Access Article. Published on 23 April 2026. Downloaded on 4/23/2026 9:19:50 PM.
This article is licensed under a Creative Commons Attribution-NonCommercial 3.0 Unported Licence.

Journal of Analytical Atomic Spectrometry Accepted Manuscript

View Article Online
DOI: 10.1039/D6JA00062B

This situation is clearly much more complex than the CaF investigated before, with so many peaks that can appear at different spectral wavelengths. Therefore, in this case, more powerful data processing approaches are required to extract the isotopic information.

The use of machine learning was hence investigated. An artificial neural network (ANN) was selected. ANNs are an excellent choice for regression problems because they can model complex, nonlinear relationships between inputs and continuous outputs. In addition, their implementation is highly portable across different machine learning environments and frameworks, enabling models to be trained, deployed, and reproduced consistently on diverse platforms.

To test the validity of the model developed, combinations with different abundances of isotopes ^{40}Ca and ^{44}Ca, together with isotopes ^{35}Cl and ^{37}Cl were prepared and measured, as described in section 2.4. In total, 121 isotopic combinations were measured in quintuplicate on four different days. Due to data variability, each spectrum was blank-corrected and normalized to the maximum peak height. Of the different spectra obtained from each measurement (one approximately every 0.073 seconds), only the ones giving rise to the maximum signal (1, 3, or 5 spectra) were considered to minimize the influence of the noise. The differences observed when varying the number of spectra selected are minimal, but the results appear slightly better with 5 spectra; thus, only the results for this scenario will be reported.

Given the small size of the training dataset, a small model has also been selected to prevent overfitting. The model was developed using the MLPRegressor from the sklearn.neural_network library with the following hyperparameters:

1) Preprocessing: each spectrum was blank-corrected and normalized to the maximum peak height.

Open Access Article. Published on 23 April 2026. Downloaded on 4/23/2026 9:19:50 PM.
This article is licensed under a Creative Commons Attribution-NonCommercial 3.0 Unported Licence.

Journal of Analytical Atomic Spectrometry Accepted Manuscript

View Article Online
DOI: 10.1039/D6JA00062B

2) ANN architecture: Inputs: 605. Hidden layers: [64, 32, 32, 16], solver = 'adam', LR= ‘constant’, learning_rate='constant', learning_rate_init= 0.005, alpha = 10e-3, early_stopping = True, activation='relu', maximum number of iterations = 10000, alpha = 10e-3. Other hyperparameters used the default library values.

To further reduce overfitting and improve accuracy and robustness, an ensemble of 50 ANNs was used. With this approach, the ensemble combines multiple perspectives, leading to more accurate and reliable predictions than any single model. In addition, the divergences among the models' predictions can be used to estimate the uncertainty of the generated output. In a regression problem, uncertainty can be measured by examining the distribution of predictions produced by the ensemble of models: the mean represents the final prediction, whereas the standard deviation across the ensemble quantifies predictive uncertainty, with a larger deviation indicating lower confidence in the prediction. Including uncertainty estimates increases trust and transparency in machine learning models. If, for a given input, very similar predictions are obtained across all models, this indicates that uncertainty is very low and, hence, the predictions are robust and reliable; conversely, a high uncertainty denotes that the predictions are not truly reliable.

A cross-validation approach has been followed for the training process. By repeatedly training and evaluating the model on different data splits, cross-validation reduces dependence on a single train–test split and helps detect overfitting. It also makes better use of limited data and yields performance estimates that are less biased and more representative of the model’s performance on unseen data. Since we had 121 different experiments, we trained 121 ensembles of 50 ANNs, each trained on 120 of the 121 experiments and tested on the unseen experiment.

Open Access Article. Published on 23 April 2026. Downloaded on 4/23/2026 9:19:50 PM.
This article is licensed under a Creative Commons Attribution-NonCommercial 3.0 Unported Licence.

Journal of Analytical Atomic Spectrometry Accepted Manuscript

View Article Online
DOI: 10.1039/D6JA00062B

Open Access Article. Published on 23 April 2026. Downloaded on 4/23/2026 9:19:50 PM.
This article is licensed under a Creative Commons Attribution-NonCommercial 3.0 Unported Licence.

This is a demanding scenario, given that each input data point corresponds to a distinct combination of isotope abundances, and therefore, when one of them is removed, the ANN model has no information about that region of input values. The aim of this approach is to assess whether the model is capable of generalizing the information learned during training and applying it to make accurate predictions in unknown regions. Neural networks are generally effective at learning patterns that enable them to generalize well to unseen data when such data follow similar distributions and underlying rules to those in the training set. However, their performance can degrade when new data are highly noisy or governed by mechanisms different from those learned during training. With our experimental setup, we will be able to identify which regions of the analyzed input data exhibit regular behavior and are therefore well predicted by our models, and which exhibit anomalies, thereby degrading the quality of our predictions.

Since each experiment has been repeated five times, there are five predictions characterized by their mean value and standard deviation. These values can be easily combined by calculating their mean value, but slightly better results are obtained if the uncertainty represented by the standard deviation is incorporated to compute a weighted mean. Starting from the 5 measurements, each one with its mean (μ) and its standard deviation (σ), the weighted mean (μ_{final}) and the combined standard deviation (σ_{final}) are computed using the following equations:

$$w_i = \frac{1}{\sigma_i^2}$$

$$\mu_{final} = \frac{\left(\sum_{i=1}^{5} w_i \mu_i\right)}{\left(\sum_{i=1}^{5} w_i\right)}$$

Journal of Analytical Atomic Spectrometry Accepted Manuscript

View Article Online
DOI: 10.1039/D6JA00062B

$$\sigma_final = \sqrt{\frac{1}{\sum_{i=1}^{5} w_i}}$$

Table 3 summarizes several relevant performance metrics for our MLP (multilayer perceptron) model. The regression model demonstrates strong overall performance, with a very high coefficient of determination (R^2 = 0.9974), indicating that it explains nearly all of the variance in the target variable. The low mean absolute error (MAE = 0.0092) indicates that, on average, the model's predictions are very close to the observed values in absolute terms. While the mean absolute percentage error (MAPE = 22.7%) appears relatively high, the much lower median absolute percentage error (MdAPE = 1.21%) indicates that this elevated MAPE is likely driven by a small number of observations with large relative errors, rather than poor performance across most of the data. Overall, these metrics indicate that the model is accurate in most cases, with a few outliers skewing the percentage-based error measure. If the predictions for Ca and Cl are analyzed separately, the quality of the results is very similar for all metrics, but for MAPE (MAPE_Ca=12.1%, MAPE_Cl=33.2%). The higher MAPE for Cl compared to Ca, despite similar MdAPE values, indicates that a small number of Cl outliers have much larger relative errors, which disproportionately inflate the mean percentage error without affecting the typical (median) performance.

Figure 8 presents the final results, comparing the expected value with the model prediction. As the small MAE indicated, there is generally good agreement between the expected and predicted values. However, the prediction is not homogeneous. Extreme values, those with a low-abundance isotope and therefore appearing at the four edges of **Figure 8a**, are much more difficult to predict efficiently. As a rule, when an isotope's abundance is 10% or lower, predictive capability declines significantly. This is certainly not unexpected, as the contribution of minor isotopes to the overall

Open Access Article. Published on 23 April 2026. Downloaded on 4/23/2026 9:19:50 PM.
This article is licensed under a Creative Commons Attribution-NonCommercial 3.0 Unported Licence.

Journal of Analytical Atomic Spectrometry Accepted Manuscript

View Article Online
DOI: 10.1039/D6JA00062B

signal becomes less evident and can be masked by other sources of uncertainty (e.g. blank contribution, noise level). This is why outliers generate high mean MAPE values. If a model works well most of the time but there are situations in which the error is very large, it is essential that the model itself be able to detect these situations and warn when its predictions are not reliable. As explained before, our model includes 50 different MLPs, and each experiment has been carried out five times. Hence, our prediction is constructed from 5x50 predictions, which allows us to calculate the standard deviation of both the models and the experiments and use it to detect predictions with high uncertainty. In fact, there is a high correlation (r^2=0.882) between the coefficient of variation (CV, defined as the ratio of the standard deviation to the mean) and the MAPE. This can be observed in **Figure 8b**, which presents both metrics for each prediction.

This correlation is useful, since it could serve to set limits, such that values exceeding a certain CV can be considered unreliable and investigated in greater detail and/or remeasured. For example, if a 0.05 CV threshold is used to select only the most reliable predictions, 100 of the 121 predictions will be selected, and their MAPE will be reduced from the original 22.7% to 2.5% only. This demonstrates the usefulness of enriching predictions with measures of uncertainty, such as the standard deviation or the CV, although in a real-world deployment, this threshold must be determined through an independent validation set to avoid over-optimistic results.

To further test the model once developed, additional samples measured on a different day were evaluated. These samples have never been seen by the model, providing more information about its performance with absolute unknowns.

The results are shown in **Figure 9a**. Again, the same conclusions can be obtained. The MAE is again very small, on average 0.0098, but the MAPE is again high, on

Open Access Article. Published on 23 April 2026. Downloaded on 4/23/2026 9:19:50 PM.
This article is licensed under a Creative Commons Attribution-NonCommercial 3.0 Unported Licence.

Journal of Analytical Atomic Spectrometry Accepted Manuscript

View Article Online
DOI: 10.1039/D6JA00062B

average 35.0%, due to the occurrence of outliers, especially in the lower-right corner. Since there are few measurements, the weight of these outliers is greater. However, these anomalous situations can be identified by the strong correlation between MAPE and CV, as shown in **Figure 9b**.

Overall, these results demonstrate the potential of machine learning strategies to enable the simultaneous calculation of the isotopic abundances of the two elements comprising the molecule using high-resolution CS GFMAS. This feature is reported for the first time with this technique and is uncommon even when using other techniques more dedicated to isotopic analysis, although it has been reported before for LAMIS (e.g., Mao et al. reported the simultaneous isotopic measurements of hydrogen and oxygen with LAMIS).[29] Nevertheless, the methodology shows some limitations, particularly when low-abundance isotopes are present, such that the accuracy of predictions for ratios above 8 or below 0.12 (for both elements) is significantly reduced. In these situations, it is particularly important to have well-calibrated uncertainty estimates, which allow us to identify when we can trust model predictions and when the margin of error is likely to be very high.

4. Conclusions

This work explores different approaches for the selection and processing of isotopic data *via* HR CS GFMAS, using two very different molecular systems as a proof of concept: CaF and CaCl. It is demonstrated that there is potential for improvement in simple situations (CaF: two separate peaks for two different Ca isotopes that can always be monitored at the same wavelengths), for instance, by using the regression approach, leading to RSD values in the 0.5-1.0% range.

On the other hand, it is also shown that much more complex situations (CaCl: various peaks that appear at different wavelengths as a result of the varying isotopic

Open Access Article. Published on 23 April 2026. Downloaded on 4/23/2026 9:19:50 PM.
This article is licensed under a Creative Commons Attribution-NonCommercial 3.0 Unported Licence.

Journal of Analytical Atomic Spectrometry Accepted Manuscript

View Article Online
DOI: 10.1039/D5JA00062B

composition of both Ca and Cl) can also be tackled by making use of machine learning, enabling the dual isotopic analysis of both elements giving rise to the target molecule, albeit with limitations in accuracy when one of the isotopes shows a low abundance. It is also worth noting that computing the prediction uncertainty can help flag potentially inaccurate results, thereby increasing the model's robustness.

It is also necessary to state that, while the previous literature demonstrates that isotope analysis *via* HR CS GFMAS is applicable to a variety of samples (biological, environmental, polymeric), this aspect was not investigated in the current work and, thus, should be further tested.

Data availability

Data is available through Zenodo (doi:10.5281/zenodo.19485273). The MLP model used is available through GitHub's University of Zaragoza repository: https://github.com/universidad-zaragoza/Ca-isotopic-analysis-via-ICP-MS-with-ML.

Conflicts of interest

The authors declare no competing financial interests.

Acknowledgments

The authors are grateful to projects PID2024-156411NB-I00, PID2022-136454NB - C22, and PID2021-122455NB-I00 (funded by MICIU/AEI/10.13039/501100011033 and by ERDF) and to the Aragon Government (Grupo E43_20R). André L. M. de Souza also acknowledges MCIN/AEI/10.13039/501100011033 for his predoctoral grant (PRE2019-091118).

References

1 M. Resano, M. Aramendía, F. V. Nakadi, E. García-Ruiz, C. Alvarez-Llamas, N. Bordel, J. Pisonero, E. Bolea-Fernández, T. Liu and F. Vanhaecke, *Trends Anal. Chem.*, 2020, **129**, 115955.

Open Access Article. Published on 23 April 2026. Downloaded on 4/23/2026 9:19:50 PM.
This article is licensed under a Creative Commons Attribution-NonCommercial 3.0 Unported Licence.

Journal of Analytical Atomic Spectrometry Accepted Manuscript

View Article Online
DOI: 10.1039/D6JA00062B

2 B. Welz, M. G. R. Vale, S. Florek, M. Okruss, M. D. Huang, H. Becker-Ross and M. Resano, High-Resolution Continuum Source Atomic Absorption Spectrometry – Theory and Applications, in *Encyclopedia of Analytical Chemistry*, ed. R. A. Meyers, Wiley, Chichester, 1st edn., 2024.

3 U. Heitmann, H. Becker-Ross, S. Florek, M. D. Huang and M. Okruss, *J. Anal. At. Spectrom.*, 2006, **21**, 1314–1320.

4 M. Resano, M. R. Flórez and E. García-Ruiz, *Anal. Bioanal. Chem.*, 2014, **406**, 2239–2259.

5 L. R. R. Souza, *Anal. Lett.*, 2021, **54**, 2574–2589

6 B. Welz, F. G. Lepri, R. G. O. Araujo, S. L. C. Ferreira, M. D. Huang, M. Okruss and H. Becker-Ross, *Anal. Chim. Acta*, 2009, **647**, 137–148.

7 B. Welz, S. Morés, E. Carasek, M. G. R. Vale, M. Okruss and H. Becker-Ross, *Appl. Spectrosc. Rev.*, 2010, **45**, 327–354.

8 F. V. Nakadi, A. Garcia-Garcia, A. Rua-Ibarz and M. Resano, *Talanta*, 2025, **292**, 127920.

9 X. Mao, A. A. Bol'shakov, I. Choi, C. P. McKay, D. L. Perry, O. Sorkhabi and R. E. Russo, *Spectrochim. Acta Part B*, 2011, **66**, 767–775.

10 A. A. Bol'shakov, X. Mao, J. J. Gonzalez and R. E. Russo, *J. Anal. At. Spectrom.*, 2016, **31**, 119–134.

11. C. G. Parigger, D. M. Surmick, C. M. Helstern, G. Gautam, A. A. Bol'shakov, R.E. Russo, in *Laser-Induced Breakdown Spectroscopy*, edited by Jagdish P. Singh, and Surya N. Thakur, Elsevier, Second Edition, 2020, Molecular laser-induced breakdown Spectroscopy, 167–209.

12 H. Wiltsche, K. Prattes, M. Zischka and G. Knapp, *Spectrochim. Acta Part B*, 2009, **64**, 341–346.

Open Access Article. Published on 23 April 2026. Downloaded on 4/23/2026 9:19:50 PM.
This article is licensed under a Creative Commons Attribution-NonCommercial 3.0 Unported Licence.

Journal of Analytical Atomic Spectrometry Accepted Manuscript

View Article Online
DOI: 10.1039/D6JA00062B

13 A. Winckelmann, S. Nowak, S. Richter, S. Recknagel, J. Riedel, J. Vogl, U. Panne and C. Abad, *Anal. Chem.*, 2021, **93**, 10022–10030.

14 F. V. Nakadi, M. A. M. S. Da Veiga, M. Aramendía, E. García-Ruiz and M. Resano, *J. Anal. At. Spectrom.*, 2015, **30**, 1531–1540.

15 F. V. Nakadi, M. A. M. S. da Veiga, M. Aramendía, E. García-Ruiz and M. Resano, *J. Anal. At. Spectrom.*, 2016, **31**, 1381–1390.

16 C. Abad, S. Florek, H. Becker-Ross, M. D. Huang, H.-J. Heinrich, S. Recknagel, J. Vogl, N. Jakubowski and U. Panne, *Spectrochim. Acta Part B*, 2017, **136**, 116–122.

17 M. B. T. Zanatta, F. V. Nakadi, M. Resano and M. A. M. S. da Veiga, *J. Anal. At. Spectrom.*, 2019, **34**, 2280–2287.

18 T. Bashiri, P. Yu, N. R. Hutzler, T. C. Steimle, C. Abad and M. Okumura, *J. Mol. Spectrosc.*, 2025, **410**, 112023.

19 A. Bazo, R. Garde, E. Garcia-Ruiz, M. Aramendía, F. V. Nakadi and M. Resano, *J. Anal. At. Spectrom.*, 2022, **37**, 2517–2528.

20 M. Aramendía, A. L. M. de Souza, F. V. Nakadi and M. Resano, *J. Anal. At. Spectrom.*, 2024, **39**, 767–779.

21 C. Abad, D. Jegielka, A. Aloysius and S. Recknagel, *J. Anal. At. Spectrom.*, 2025, **40**, 2692–2701.

22 J. Fietzke, M. Frische, T. H. Hansteen and A. Eisenhauer, *J. Anal. At. Spectrom.,* 2008, **23**, 769–772.

23 J. Fietzke, V. Liebetrau, D. Gunther, K. Gürs, K. Hametner, K. Zumholz, T. H. Hansteen and A. Eisenhauer, *J. Anal. At. Spectrom.,* 2008, **23**, 955–961.

24 R. W. B. Pearse and A. G. Gaydon, *The Identification of Molecular Spectra,* Chapman & Hall, London, 3rd edn., 1963.

Open Access Article. Published on 23 April 2026. Downloaded on 4/23/2026 9:19:50 PM.
This article is licensed under a Creative Commons Attribution-NonCommercial 3.0 Unported Licence.

Journal of Analytical Atomic Spectrometry Accepted Manuscript

View Article Online
DOI: 10.1039/D6JA00062B

25 A. Guarda, M. Aramendía, I. Andrés, E. García-Ruiz, P. C. do Nascimento and M. Resano, *Talanta*, 2017, **162**, 354–361.

26 G. Herzberg, *Molecular Spectra and Molecule Structure I. Spectra of Diatomic Molecules,* D. Van Nostrand Company Inc., Princeton, 2nd edn., 1950.

27 U. Heitmann, B. Welz, D. L. G. Borges and F. Lepri, *Spectrochim. Acta Part B*, 2007, **62**, 1222–1230.

28 M. Resano, A. C. Lapeña and M. A. Belarra, *Anal. Methods*, 2013, **5**, 1130–1139.

29 X. Mao, D.L. Perry, A. A. Bol'shakov, R.E. Russo, *Spectroscopy*, 2014, **29**.

Open Access Article. Published on 23 April 2026. Downloaded on 4/23/2026 9:19:50 PM.
This article is licensed under a Creative Commons Attribution-NonCommercial 3.0 Unported Licence.

Journal of Analytical Atomic Spectrometry Accepted Manuscript

View Article Online
DOI: 10.1039/D6JA00062B

Figure captions

Figure 1. Wavelength- and time-resolved signal obtained by HR CS GFMAS using the conditions shown in **Table 1** when monitoring a solution containing approximately 5 μg of ^{40}Ca and 5 μg of ^{44}Ca in the presence of an excess of F (0.5 mg of NaF). 2D projections on the Z-axis are also displayed to show the wavelength-integrated and time-integrated signals. The absorbance was normalized to a maximum value of 2 to keep all the values on the same scale.

Figure 2. Time-integrated signals obtained by HR CS GFMAS using the conditions shown in **Table 1** when monitoring a solution containing approximately 5 μg of ^{40}Ca and 5 μg of ^{44}Ca in the presence of an excess of F (0.5 mg of NaF). **A)** Absorbance signal of the first ^{40}CaF peak (around 515.2 nm) and RSD values obtained at each detector pixel (n=15); **B)** Absorbance signal of the first ^{44}CaF peak (around 515.4 nm) and RSD values obtained at each detector pixel (n=15); **C)** Signal ratios using each pair of detector pixels from A and B, with the corresponding RSD values. Error bars represent the standard deviation.

Figure 3. Wavelength-integrated signals (1 detector pixel) obtained by HR CS GFMAS using the conditions shown in **Table 1** when monitoring a solution containing approximately 5 μg of ^{40}Ca and 5 μg of ^{44}Ca in the presence of an excess of F (0.5 mg of NaF). **A)** Absorbance temporal profile of the first ^{40}CaF peak (around 515.2 nm) and RSD values for each spectrum collected (n=15); **B)** Absorbance temporal profile of the first ^{44}CaF peak (around 515.4 nm) and RSD values for each spectrum collected (n=15); **C)** Signal ratios using each spectrum from A and B, with the corresponding RSD values. Error bars represent the standard deviation.

Figure 4. A) Wavelength-integrated signals (1 detector pixel) obtained by HR CS GFMAS using the conditions shown in **Table 1** when monitoring a solution containing

Open Access Article. Published on 23 April 2026. Downloaded on 4/23/2026 9:19:50 PM.
This article is licensed under a Creative Commons Attribution-NonCommercial 3.0 Unported Licence.

Journal of Analytical Atomic Spectrometry Accepted Manuscript

View Article Online
DOI: 10.1039/D5JA00062B

approximately 5 μg of ^{40}Ca and 5 μg of ^{44}Ca in the presence of an excess of F (**0.5** mg of NaF), showing the absorbance temporal profile of the first ^{40}CaF peak (around 515.2 nm) and the first ^{44}CaF peak (around 515.4 nm). The central 10 peak points are highlighted. **B)** Example of the regression approach using all the points acquired in A, whereas the $^{44}Ca/^{40}Ca$ ratio corresponds to the slope estimated for the calibration curve.

Figure 5. Precision, expressed as RSD%, obtained by HR GFMAS for $CaCO_3$ solutions prepared with different $^{44}Ca/^{40}Ca$ ratios, with different overall Ca contents, and processing the data using either 1, 3, or 5 detector pixels and a different procedure to evaluate the peak temporal profile (either the regression approach, as shown in **Figure 4** and indicated as slope, or a number of peak pixels of 1, 3, 5 or 10). **A)** $^{44}Ca/^{40}Ca$ ratio of approx. 1; **B)** $^{44}Ca/^{40}Ca$ ratio of approx. 0.25; **C)** $^{44}Ca/^{40}Ca$ ratio of approx. 4.

Figure 6. Experimental ratio $^{44}Ca/^{40}Ca$ obtained by HR CS GFMAS divided by the reference $^{44}Ca/^{40}Ca$ ratio (measured by ICP-MS) for solutions prepared with different $^{44}Ca/^{40}Ca$ ratios, with different overall Ca contents, and processing the data using either 1, 3, or 5 detector pixels and a different procedure to evaluate the peak temporal profile (either the regression approach, as shown in **Figure 4**, or a number of peak pixels of 1, 3, 5 or 10). **A)** $^{44}Ca/^{40}Ca$ ratio of approx. 1; **B)** $^{44}Ca/^{40}Ca$ ratio of approx. 0.25; **C)** $^{44}Ca/^{40}Ca$ ratio of approx. 4.

Figure 7. Time-integrated and 2D wavelength-resolved spectra of CaCl with different isotopic compositions obtained by HR CS GFMAS, normalized to the highest spectrum value, using conditions shown in **Table 2**. The total mass for both Ca and Cl in each spectrum is 1.8 μg. The first five peaks of each pure spectrum, obtained with a value close to100% for each Ca and Cl isotope present, are identified as 1 to 5.

Open Access Article. Published on 23 April 2026. Downloaded on 4/23/2026 9:19:50 PM.
This article is licensed under a Creative Commons Attribution-NonCommercial 3.0 Unported Licence.

Journal of Analytical Atomic Spectrometry Accepted Manuscript

View Article Online
DOI: 10.1039/D6JA00062B

Figure 8. A) Expected and predicted values for the mixtures of different Cl and Ca isotopic composition measured by HR CS GFMAS, using the MLP model described in section 3.3. **B)** Correlation between the mean absolute percentage error and the coefficient of variation of the predictions shown in A.

Figure 9. A) Expected and predicted values for two series of mixtures of different Ca and Cl isotope compositions, which were completely unknown to the MLP model. **B)** Correlation between the mean absolute percentage error and the coefficient of variation of the predictions shown in A.

Open Access Article. Published on 23 April 2026. Downloaded on 4/23/2026 9:19:50 PM.
This article is licensed under a Creative Commons Attribution-NonCommercial 3.0 Unported Licence.

Journal of Analytical Atomic Spectrometry Accepted Manuscript

Figure 1

View Article Online
DOI: 10.1039/D6JA00062B

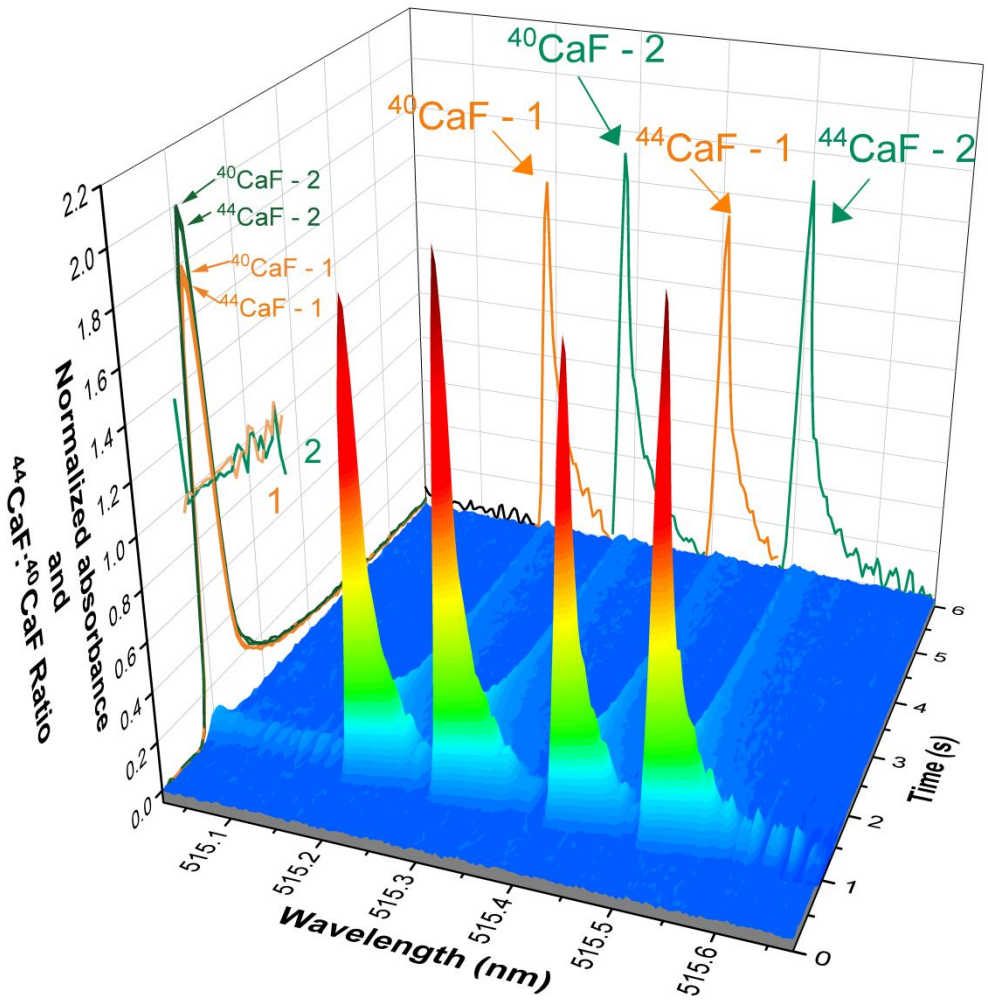

Open Access Article. Published on 23 April 2026. Downloaded on 4/23/2026 9:19:50 PM.
This article is licensed under a Creative Commons Attribution-NonCommercial 3.0 Unported Licence.

Journal of Analytical Atomic Spectrometry Accepted Manuscript

Figure 2

View Article Online
DOI: 10.1039/D6JA00062B

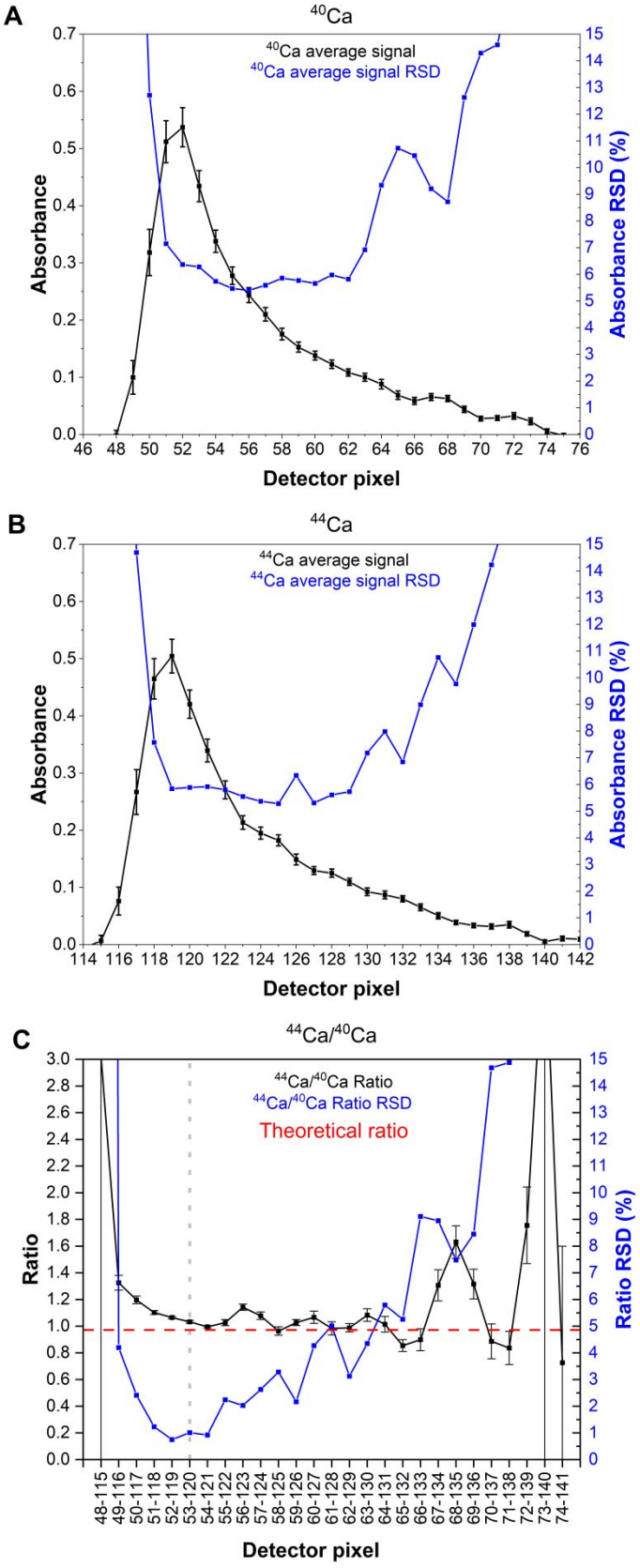

Open Access Article. Published on 23 April 2026. Downloaded on 4/23/2026 9:19:50 PM.
This article is licensed under a Creative Commons Attribution-NonCommercial 3.0 Unported Licence.

Journal of Analytical Atomic Spectrometry Accepted Manuscript

Figure 3

View Article Online
DOI: 10.1039/D6JA00062B

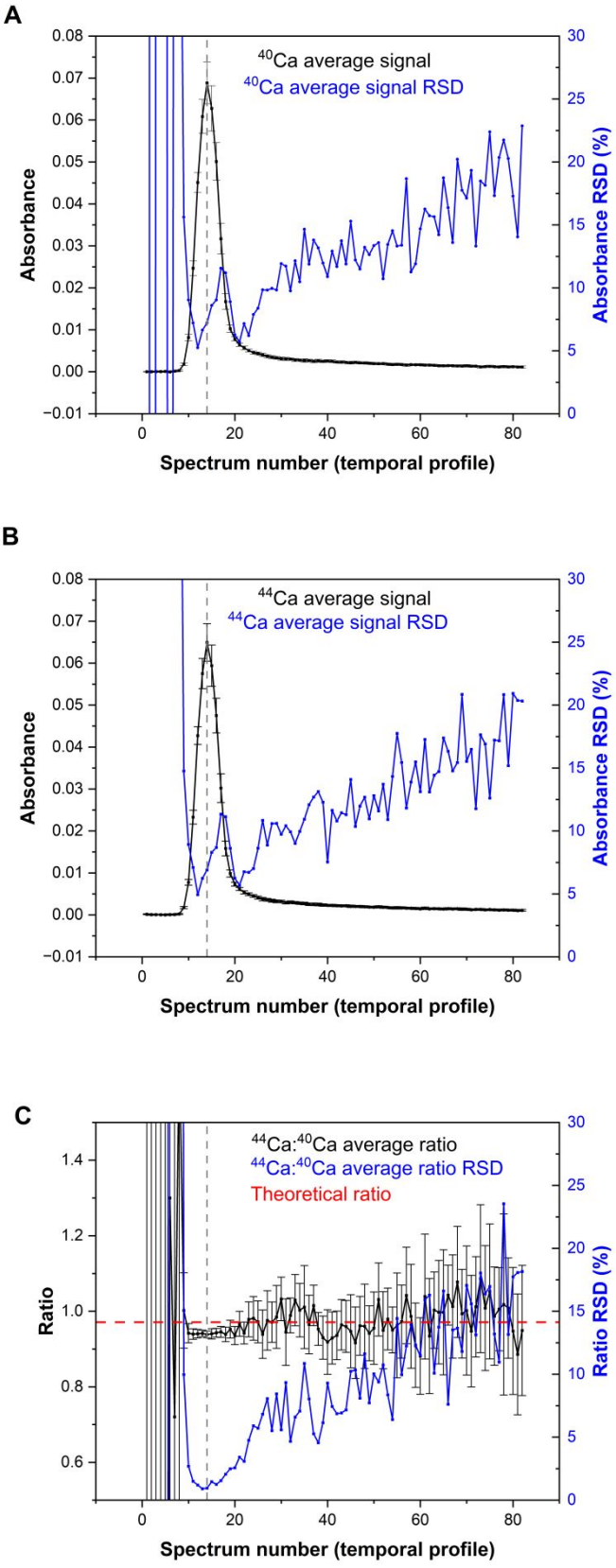

Open Access Article. Published on 23 April 2026. Downloaded on 4/23/2026 9:19:50 PM.
This article is licensed under a Creative Commons Attribution-NonCommercial 3.0 Unported Licence.

Journal of Analytical Atomic Spectrometry Accepted Manuscript

View Article Online
DOI: 10.1039/D6JA00062B

Figure 4

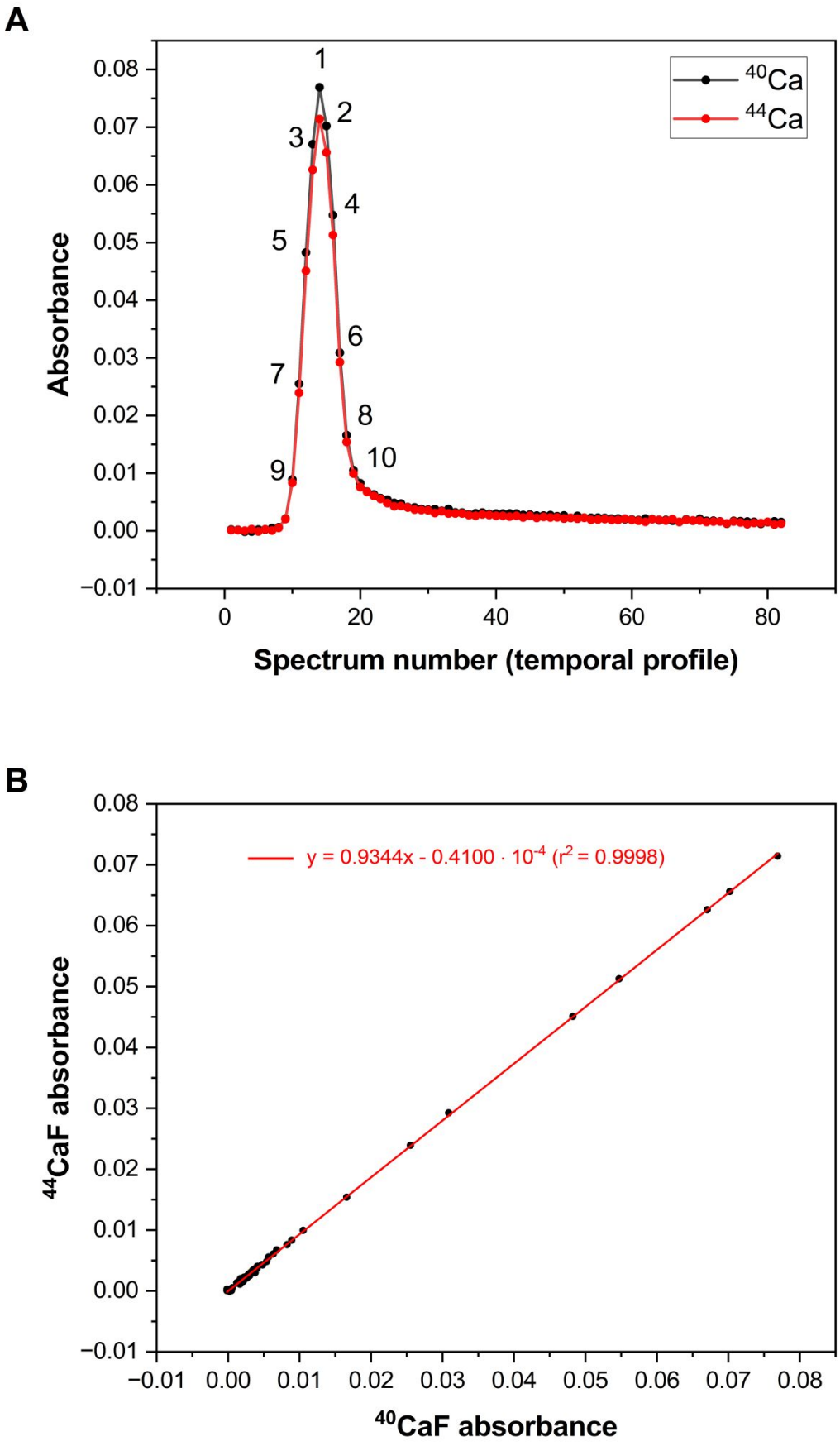

Open Access Article. Published on 23 April 2026. Downloaded on 4/23/2026 9:19:50 PM.
This article is licensed under a Creative Commons Attribution-NonCommercial 3.0 Unported Licence.

Journal of Analytical Atomic Spectrometry Accepted Manuscript

Open Access Article. Published on 23 April 2026. Downloaded on 4/23/2026 9:19:50 PM.
This article is licensed under a Creative Commons Attribution-NonCommercial 3.0 Unported Licence.

Figure 5

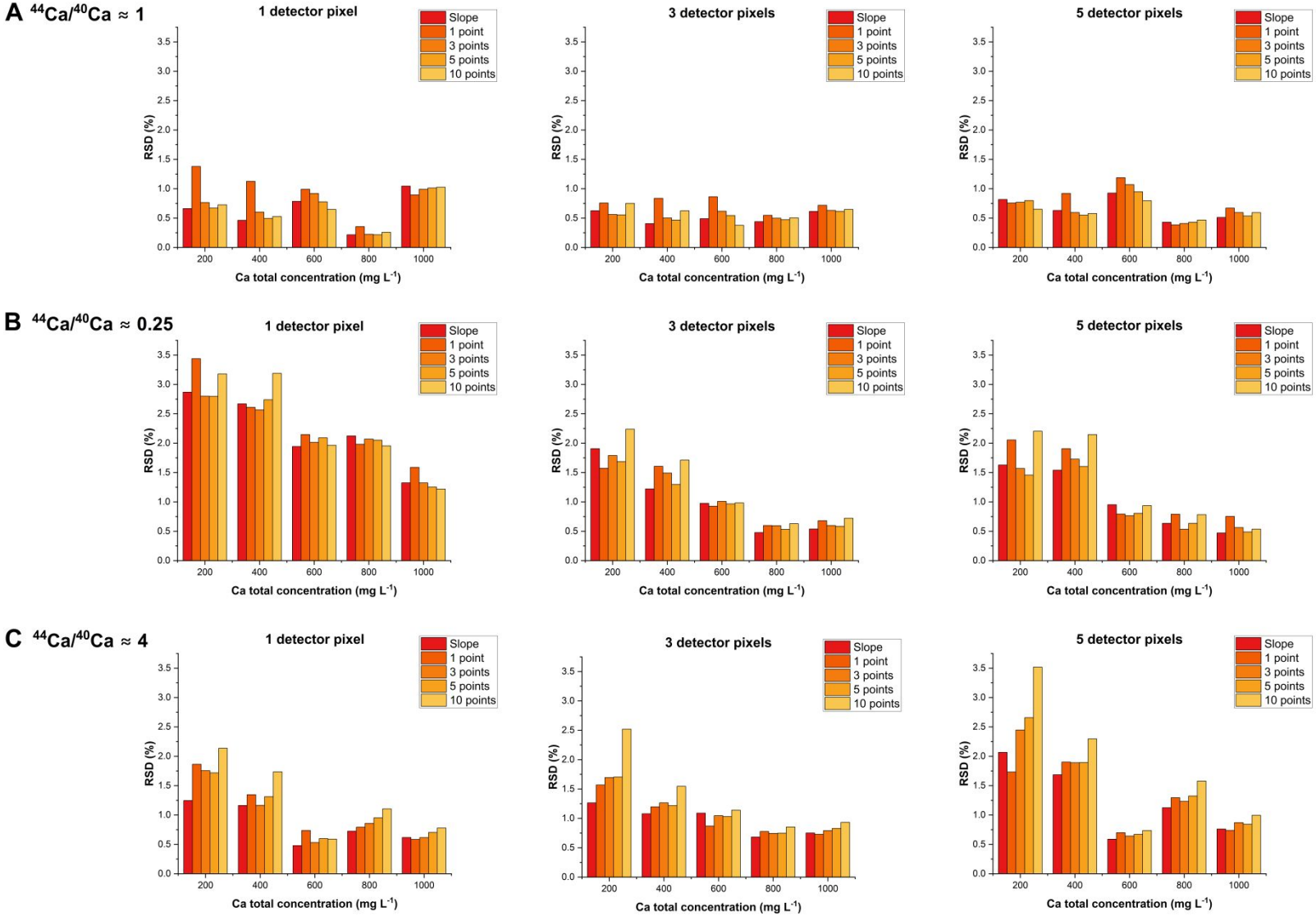

Journal of Analytical Atomic Spectrometry Accepted Manuscript

Open Access Article. Published on 23 April 2026. Downloaded on 4/23/2026 9:19:50 PM.
This article is licensed under a Creative Commons Attribution-NonCommercial 3.0 Unported Licence.

Figure 6

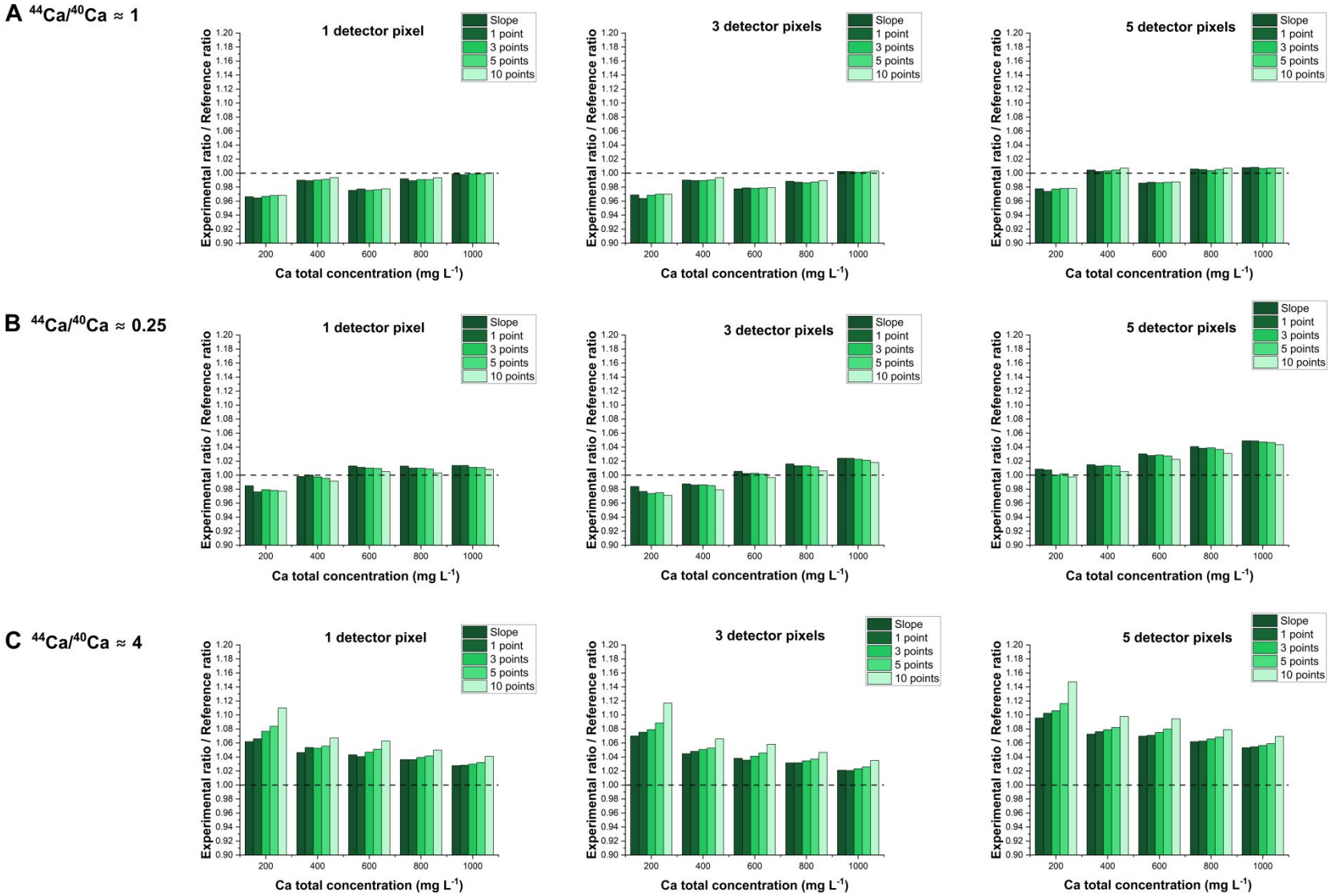

Journal of Analytical Atomic Spectrometry Accepted Manuscript

Figure 7

View Article Online
DOI: 10.1039/D6JA00062B

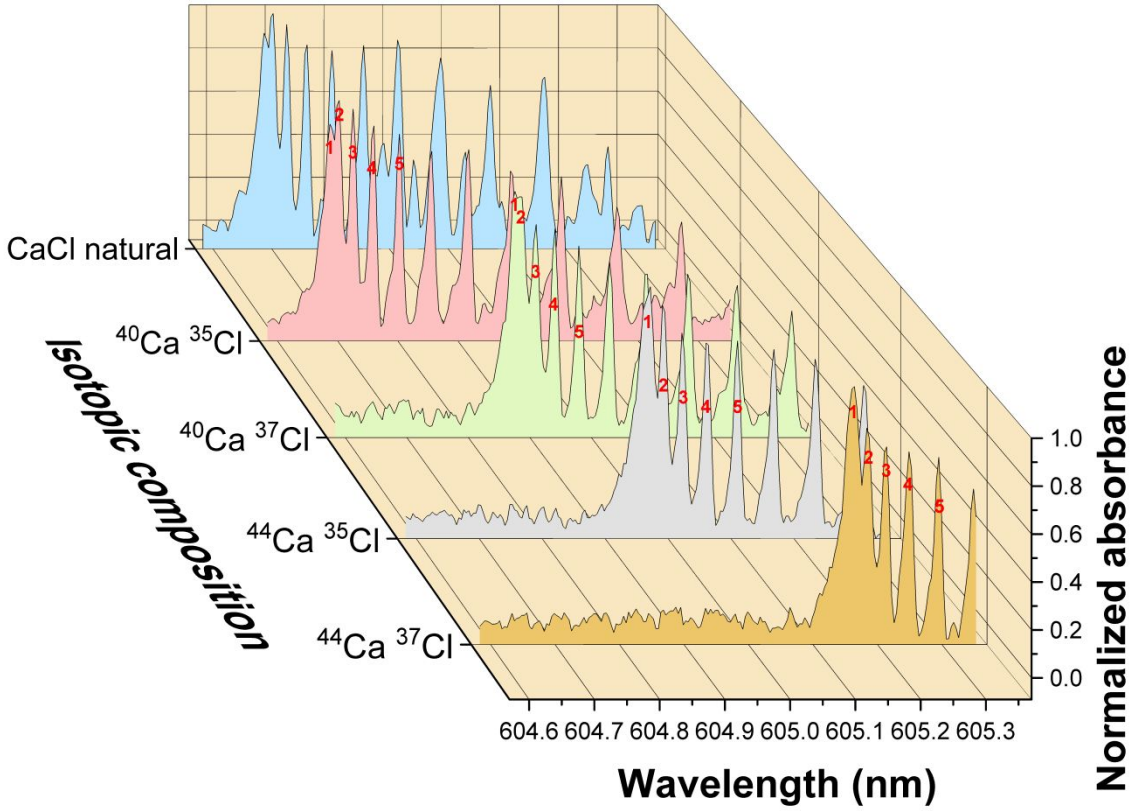

Open Access Article. Published on 23 April 2026. Downloaded on 4/23/2026 9:19:50 PM.
This article is licensed under a Creative Commons Attribution-NonCommercial 3.0 Unported Licence.

Journal of Analytical Atomic Spectrometry Accepted Manuscript

Figure 8

View Article Online
DOI: 10.1039/D6JA00062B

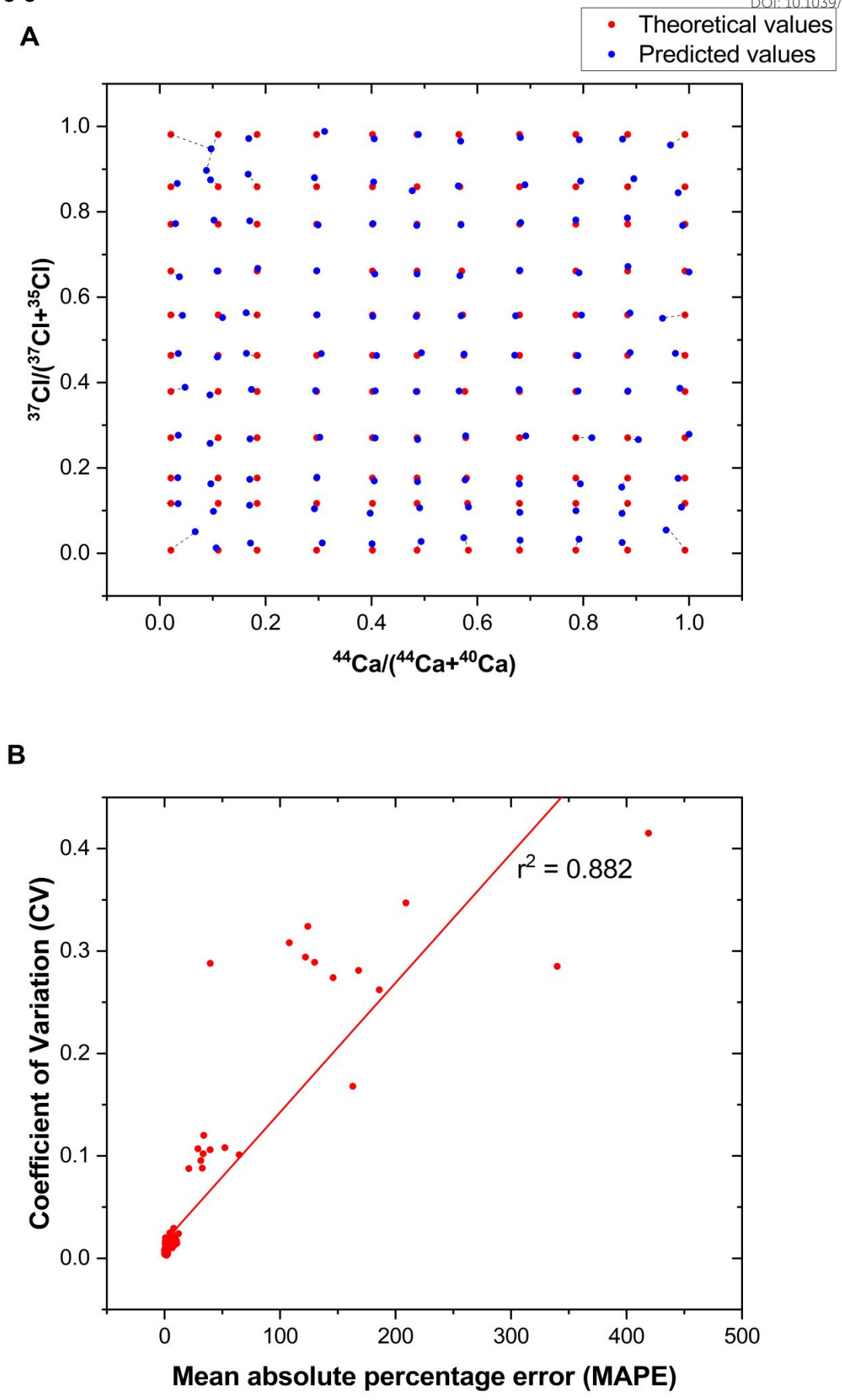

Open Access Article. Published on 23 April 2026. Downloaded on 4/23/2026 9:19:50 PM.
This article is licensed under a Creative Commons Attribution-NonCommercial 3.0 Unported Licence.

Journal of Analytical Atomic Spectrometry Accepted Manuscript

View Article Online
DOI: 10.1039/D6JA00062B

Figure 9

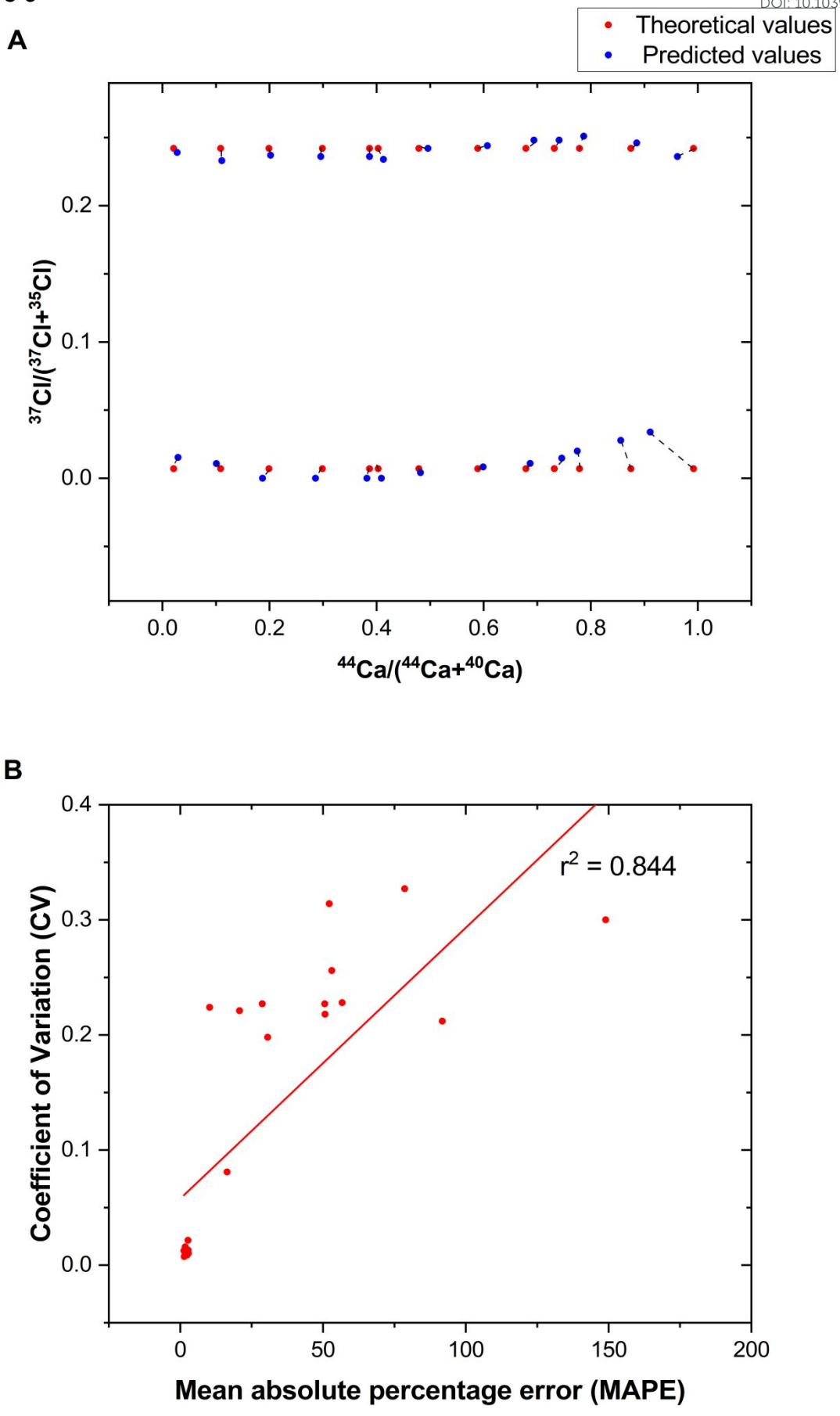

Open Access Article. Published on 23 April 2026. Downloaded on 4/23/2026 9:19:50 PM.
This article is licensed under a Creative Commons Attribution-NonCommercial 3.0 Unported Licence.

Journal of Analytical Atomic Spectrometry Accepted Manuscript

View Article Online
DOI: 10.1039/D6JA00062B

Table 1. Instrumental parameters for CaF measurements by HR CS GFMAS.

Electronic transition	$B^2\Sigma$-$X^2\Sigma$
Wavelengths	515.350 nm (central pixel 101)
	515.190 nm (^{40}CaF)
	515.408 nm (^{44}CaF)
Fluorinating agent	10 μL of NaF 5% m v^{-1}
Aqueous sample volume	10 μL
Ca mass introduced	2 – 10 μg
^{44}Ca/^{40}Ca isotopic ratio	4:1, 1:1 and 1:4
Measurement time	6 s

Temperature program

Step	Temperature (°C)	Ramp (°C s^{-1})	Hold (s)	Ar gas flow (L min^{-1})
Drying	90	3	20	2.0
Drying	110	5	20	2.0
Pyrolysis	800	300	10	2.0
Gas adaption	800	0	5	0
Vaporization	2200	3000	6	0
Cleaning	2400	1500	4	2.0

Open Access Article. Published on 23 April 2026. Downloaded on 4/23/2026 9:19:50 PM.
This article is licensed under a Creative Commons Attribution-NonCommercial 3.0 Unported Licence.

Journal of Analytical Atomic Spectrometry Accepted Manuscript

View Article Online
DOI: 10.1039/D6JA00062B

Table 2. Instrumental parameters for CaCl measurements by HR CS GFMAS.

Electronic transition	$A^2\Pi$-$X^2\Sigma$
Wavelength	604.970 nm (central pixel 101)
Standard amounts	Ca: 10 μL, 180 mg L^{-1}
	Cl: 10 μL, 180 mg L^{-1}
Isotopic compositions monitored	$^{44}Ca/^{40}Ca$: 0:1.0, 0.1:0.9, 0.2:0.8, 0.3:0.7, 0.4:0.6, 0.5:0.5, 0.6:0.4, 0.7:0.3, 0.8:0.2, 0.9:0.1, 1.0:0
	$^{37}Cl/^{35}Cl$: 0:1.0, 0.1:0.9, 0.2:0.8, 0.3:0.7, 0.4:0.6, 0.5:0.5, 0.6:0.4, 0.7:0.3, 0.8:0.2, 0.9:0.1, 1.0:0
Measurement time	5 s

Temperature program

Step	Temperature (°C)	Ramp (°C s^{-1})	Hold (s)	Ar gas flow (L min^{-1})
Drying	90	30	20	2.0
Drying	110	30	20	2.0
Pyrolysis	700	50	5	2.0
Gas adaption	700	0	5	0
Vaporization	2200	3000	5	0
Cleaning	2600	100	4	2.0

Open Access Article. Published on 23 April 2026. Downloaded on 4/23/2026 9:19:50 PM.
This article is licensed under a Creative Commons Attribution-NonCommercial 3.0 Unported Licence.

Journal of Analytical Atomic Spectrometry Accepted Manuscript

View Article Online
DOI: 10.1039/D6JA00062B

Table 3. Evaluation of the machine learning model predictions

	Ca	Cl	Mean
Mean absolute error (MAE)	0.0090	0.0095	0.0092
Mean absolute percentage error (MAPE)	12.1%	33.2%	22.7%
Median Absolute Percentage Error (MdAPE)	1.20%	1.22%	1.21%
R^2 (coefficient of determination)	0.9973	0.9974	0.9974

Open Access Article. Published on 23 April 2026. Downloaded on 4/23/2026 9:19:50 PM.
This article is licensed under a Creative Commons Attribution-NonCommercial 3.0 Unported Licence.

Journal of Analytical Atomic Spectrometry Accepted Manuscript

View Article Online
DOI: 10.1039/D6JA00062B

Data availability

Data is available through Zenodo (doi: 10.5281/zenodo.19485273). The MLP model used is available through GitHub's University of Zaragoza repository: https://github.com/universidad-zaragoza/Ca-isotopic-analysis-via-ICP-MS-with-ML.

Open Access Article. Published on 23 April 2026. Downloaded on 4/23/2026 9:19:50 PM.
This article is licensed under a Creative Commons Attribution-NonCommercial 3.0 Unported Licence.

Journal of Analytical Atomic Spectrometry Accepted Manuscript